MATERIALS SCIENCE

# An intelligent, compact wearable pressure-strain combo sensor system for continuous fetal movement monitoring

**Lim Wei Yap[1]†, Arie Levin[2]†, Yiwen Jiang[3]†, Duong Nhu[3], Shu Gong[2], Ritesh Warty[4], David Vera Anaya[2], Qinhao Li[1], Yan Lu[1], Rui Gao[1], Xin Zhang[3], Talha Ilyas[3], Vinayak Smith[4], Allison Thomas[4], Aswandi Wibrianto[1], Yuxin Zhang[2], Jane Limas[5], Sharon A. McCracken[5,6], Jonathan M. Morris[5,6], Ben W. Mol[4], Euan M. Wallace[4], Arnold Lining Ju[1], Zongyuan Ge[3]*, Faezeh Marzbanrad[7]*, Wenlong Cheng[1,2]***



**Continuous fetal movement monitoring in late pregnancy may improve fetal wellbeing and pregnancy outcomes. While fetal movements can be visualized with ultrasound, it is intermittent and limited to clinical settings. Inertial measurement units may enable at-home fetal monitoring but usually require a large-footprint, multisensor design. Here, we report smart, compact wearable pressure-strain combo sensors continuously monitoring fetal movements through maternal abdominal skin motions. In the 2D and 3D artificial abdomen systems, our octagonal-shaped gold nanowire–based strain sensor served as an isotropic sensor, enabling omnidirectional simulated "kicking load" detection within an area of ~77 (2D) and ~217 cm$^2$ (3D), while an interdigitated electrode–based pressure sensor showed highly sensitive localized load detection. Building upon these findings, we designed compact pressure- and strain-sensing integrated Band-Aids and tested on 59 pregnant women. We developed machine learning models to distinguish fetal from nonfetal movements with >90% accuracy in ultrasound-based validation studies. This AI-powered, Band-Aid–like sensing system offers potential as a compact, comfortable, and accurate continuous out-of-hospital fetal movement monitoring technology.**

## INTRODUCTION

Fetal movement (FM) is defined as a discrete kick, flutter, swish, or roll, indicative of a well-functioning central nervous system and musculoskeletal system (*1*). Reduced FM, as perceived by the mother, occurs in about 15% of pregnancies (*2*). It is a common feature in pregnancies that end in fetal death and stillbirth (*3*). A healthy term fetus typically moves in regular patterns in utero, cycling through active and quiet phases every 30 to 40 minutes (*1*). When the fetus is compromised in utero, it may reduce movements as a compensatory mechanism to conserve oxygen, which can precede stillbirth (*3*, *4*). Therefore, accurate recognition and interpretation of FM patterns are critically important for identifying fetuses at risk of stillbirth.

Despite its clinical significance, effective method of monitoring of FM remains an unmet challenge. To date, the dominant approach to day-to-day FM monitoring is largely subjective, requiring a mother to report movements experienced, termed formal fetal counting. However, 40% of FM occurs without the mother realizing it (*5*). While FM can be assessed by ultrasound imaging, it requires trained personnel and the mother to attend to a care provider. It is intermittent at best. An alternative approach is cardiotocography, where an ultrasound transducer is used to monitor fetal heart rate, and a pressure-sensitive tocodynamometer is used to monitor uterine contractions. While this can be undertaken at home and could potentially provide direct physiological signals, it requires a belt to strap the transducers, each with a large footprint size of typically ~60 to 128 cm$^2$ and ~2 to 5 cm thick, to the maternal abdomen and is also limited by being intermittent and requiring skilled personnel to read the resultant fetal heart rate tracings. Accordingly, its use is limited to only very high-risk pregnancies.

A number of FM surveillance methods are emerging, including detection of FM-induced pressure by piezoelectric sensors (*6*, *7*), FM-induced vibrations by micromechanical acoustic sensors (*8*, *9*), and measuring displacement of the maternal abdomen by accelerometers (*10*–*12*). However, these technologies often suffer from severe signal interference. For example, the environmental vibrations and noise often make it challenging to isolate fetal signals accurately (*13*). The accelerator-based method faces limitations in distinguishing maternal from FM and requires precise placement for reliable accuracy (*9*). Besides, these wearable FM monitors also require a strapping belt with a bulky footprint of ~40 to 400 cm$^2$, rendering it uncomfortable to wear.

Here, we report on an artificial intelligence (AI)–powered, compact, Band-Aid–like wearable pressure-strain combo sensor system that can continuously and accurately measure FM-induced maternal abdominal skin motions. Our devised octagonal-shaped gold nanowire film can serve as an omnidirectional strain sensor, detecting simulated fetal kicks within zones of ~77 and 217 cm$^2$ for 2D and 3D dummy systems, respectively. In contrast, the pressure sensor could detect the simulated kick more accurately but was limited

[1]School of Biomedical Engineering, Faculty of Engineering, University of Sydney, Darlington, New South Wales 2008, Australia. [2]Department of Chemical and Biological Engineering, Faculty of Engineering, Monash University, Clayton, Victoria 3168, Australia. [3]AIM for Health Lab, Faculty of Information Technology, Monash University, Clayton, Victoria, 3168, Australia. [4]Department of Obstetrics and Gynaecology, Monash University, Clayton, Victoria 3168, Australia. [5]Division of Perinatal Medicine, Faculty of Medicine and Health, University of Sydney, Kolling Institute, St. Leonards, NSW 2065, Australia. [6]Department of Obstetrics and Gynaecology, Royal North Shore Hospital, St. Leonards, NSW 2065, Australia. [7]Department of Electrical and Computer Systems Engineering, Faculty of Engineering, Monash University, Clayton, Victoria 3168, Australia.
*Corresponding author. Email: wenlong.cheng@monash.edu (W.C.); faezeh.marzbanrad@monash.edu (F.M.); zongyuan.ge@monash.edu (Z.G.)
†These authors contributed equally to this work.

within a zone of ~13 and ~38 $cm^2$ for 2D and 3D dummy systems, respectively. Building upon these findings, we designed highly compact pressure- and strain-sensing integrated Band-Aids, each with a thickness of ~3 mm, a footprint size of 10 to 14 $cm^2$ and a weight of ~3 g. With merely two Band-Aids tested on 59 gravid patients, we developed a machine learning model that could discriminate between FM and non-FM with over 90% accuracy in validation studies against ultrasound. Our intelligent Band-Aid–like sensing system indicates the potential as highly compact, comfortable yet accurate wearable technologies for monitoring FM continuously in an out-of-hospital setting.

## RESULTS

### Design principles and sensor fabrication

FM is complex, and includes kicks, rolls, and body and limb stretching of the uterus. Such fetal mechanical motions transfer mechanical loads to the maternal abdomen skin (MAS) deformation in the forms of stretching, compression, or vibration (Fig. 1A). In case of a mechanical load such as fetal kicking events, substantial MAS deformation and shift are evident as shown in the finite element analysis (FEA) (fig. S1). The fetal kicking force in the second and third trimesters of pregnancy is in the range of 29-47 N (*14*), which typically causes ~6 to 18% strain in MAS. While the commercial inertial

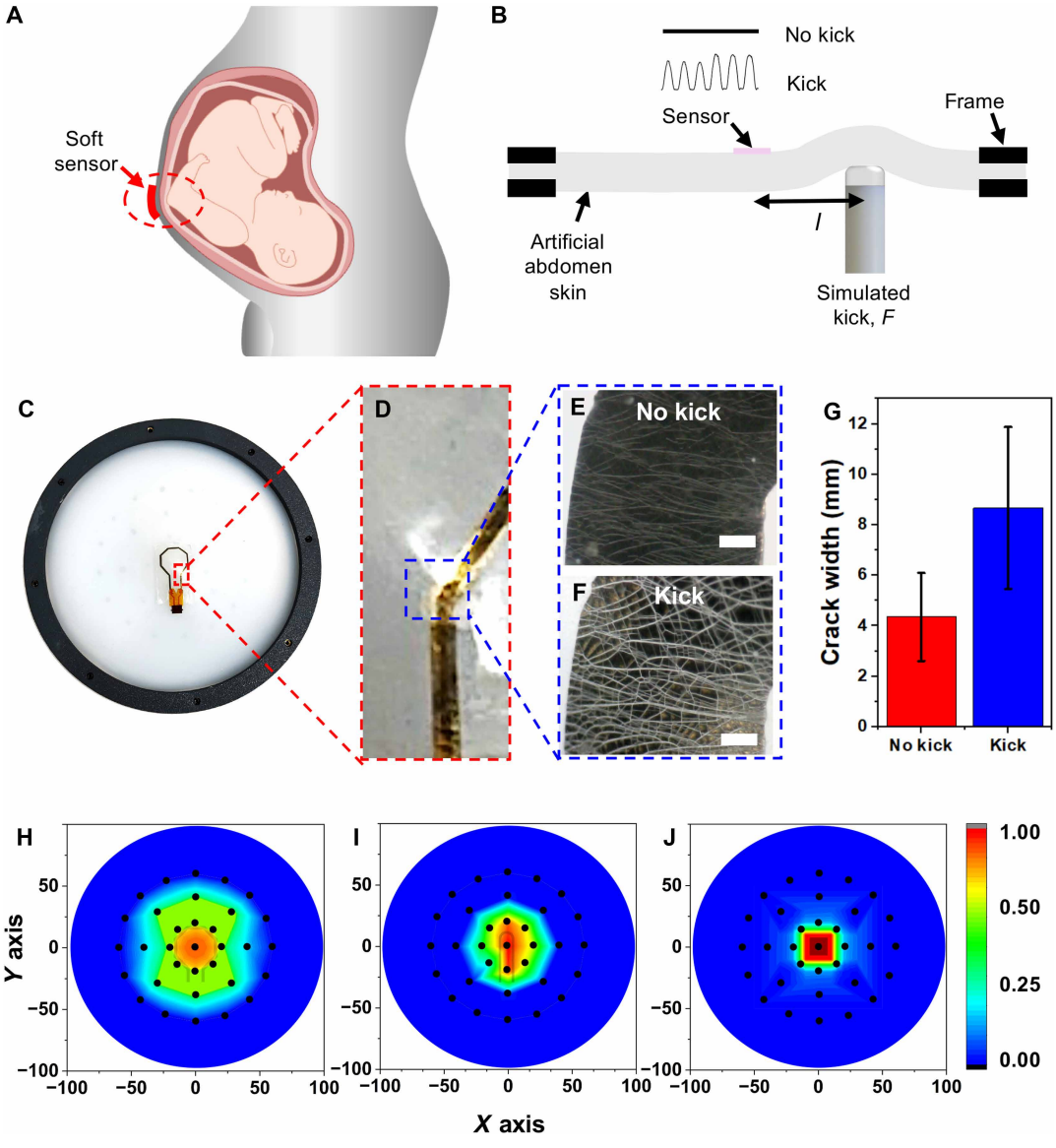


**Fig. 1. Simulated FMs in two-dimension artificial abdomen system.** (**A**) Illustration of maternal abdominal wall deformation during FMs. Image created with Microsoft PowerPoint. (**B**) Schematic illustration of fetal kick simulation toward a 2D elastomeric artificial abdomen with soft sensor mounted on the opposite side of the artificial abdomen. (**C**) Photographic image (scale bar, 5 cm) and (**D**) enlarged photographic image of Octa sensor deformation during kick simulation (scale bar, 1 mm). Microscopic image of a crack on the sensor (**E**) with no kick and (**F**) enlarged crack width during simulated kick at 15 N of force (scale bar, 200 μm). (**G**) Histogram of the crack width with no kick and simulated kick at 15 N. Pressure sensitivity heat mapping for forces applied at 27 points around the (**H**) Octa sensor, (**I**) U sensor, and (**J**) pressure sensor.

measurement unit (IMU) can detect the skin deformation, it is highly localized and will require multiple IMU sensors covering the entire MAS to capture all the possible types of FM (*10*, *11*, *15*). Such a large footprint size leads to inconvenience and discomfort. In addition, IMU will detect any interfering movement including mother's walking activities (*12*, *16*, *17*), suffering intrinsic limitations for accurate yet compact FM monitoring.

We propose the skin-conformal mechanical force sensor systems that can directly measure lateral strains and vertical pressure associated with the MAS deformation, which can be achieved with lightweight soft strain and pressure sensors, respectively. However, fetal position, sensor location, sensitivity, and detection range will determine the accuracy of FM monitoring. While multiple strain and pressure sensors may be applied to cover the entire MAS, it will lead to large footprint size with poor comfort and form factor in practical applications. Our design concept is to minimize the sensor system footprint to achieve a high accuracy in identifying FM with the fewest number of sensors possible.

We began with design, fabrication, and evaluation of soft strain and pressure sensors in detecting simulated "fetal kicking" events. To maximize the strain sensing range, an octagonal-shaped strain sensor (Octa sensor) was first devised. Unlike conventional U-shaped strain sensors, the Octa sensor can detect evenly distributed strains from omnidirectional loads owing to its design featuring seven straight edges and eight corners (fig. S2A). FEA simulation of Octa sensor attached to the maternal abdomen impacted by FM reveals that the strain from the MAS due to FM would distort the shape of the Octa sensor, particularly the vertices and corners closest to the FM site (fig. S2B). In contrast, the typical U-shaped strain sensor (U sensor) that has two long vertices and a rounded top (fig. S3A) would only experience slight distortion at the rounded edge as simulated by FEA (fig. S3B).

Our previously reported vertically aligned gold nanowires (v-AuNWs) offer reasonably high stretchability, sensitivity, and sensing range (*18*, *19*), hence, were chosen as the active materials for the fabrication of Octa- and U-sensors. Both sensors could be fabricated by shadow mask-assisted patterning growth of v-AuNWs on thin styrene-ethylene-butadiene-styrene (SEBS) substrate (fig. S4) with a final thickness of ~150 μm after sealing with Dragon Skin FX Pro. The scanning electron microscope (SEM) characterization confirmed the formation of vertically aligned gold nanowires on the SEBS substrate (fig. S5).

### Detecting of simulated fetal kicks in 2D abdomen skin

An elastomeric Ecoflex sheet of 10 mm thick was fabricated and suspended over a circular frame with a hole of 200 mm in diameter, in which our sensor was then attached to the center of suspended Ecoflex sheet on the top side (Fig. 1B). The load $F$ was applied from the bottom side of Ecoflex sheet at a distance, $l$. The sensor would record a resistive signal depending on the load and the distance to mimic the fetal kick event.

When the simulated kick was applied onto the artificial abdomen (Fig. 1, C and D), we observed the obvious local deformation accompanied by widened cracks on the Octa sensor (Fig. 1, E and F). For the ~15 N load at the corner, the crack widths were more than doubled (Fig. 1G). As expected, the widening cracks would lead to the increase in resistance, consistent with our previous report (*20*).

We then applied 33 spatial loads across various locations of the Ecoflex sheet to assess the sensors' response. The Octa sensor was able to detect simulated kicks up to a radius of ~5 cm from the center of the sensor (Fig. 1H), covering up to 24.5% of the elastomeric artificial abdomen area. The U sensor could only detect simulated kicks up to a radius of ~3.5 cm or ~12.3% of the total area of the suspended Ecoflex sheet (Fig. 1I). We also tested the response of graphite-impregnated paper-based pressure sensor with a final thickness of ~280 μm. This had a high sensitivity but localized detection to within ~2 cm radius, equivalent to ~4% area of the suspended Ecoflex sheet (Fig. 1J).

We tested three different sizes of octagon, ranging from 12.66 mm by 12.66 mm to 30 mm by 30 mm, to determine the optimal Octa sensor size and sensitivity. A 21.66 mm by 21.66 mm Octa sensor was selected as it offers balanced trade-off between sensitivity of FM and comfortable daily application (fig. S6). The strain sensitivity of the Octa sensor was also further optimized by varying the AuNW growth time between 1 and 10 min (fig. S7A). Three minutes of AuNWs growth time with nanowires length of ~480 nm (fig. S7B) was found to be the optimal trade-off between strain sensitivity and dynamic range.

We compared sensitivities of various sensors, including the Octa sensor, U sensor, and a pressure sensor (fabrication method illustrated in fig. S8), in response to a force range of ~1 to 31 N applied to their centers (figs. S9 to S11). The sensitivity to pressure is defined as $S = (\Delta R/R_o)/N$, where $\Delta R$ is the relative change in resistance, $R_o$ is the resistance of the sensor under no load, and $N$ is the applied load. The Octa sensor exhibited linear sensitivity of ~2.1 $N^{-1}$ at a small force range of ~1 to 7 N, and then the linear sensitivity decreased to ~0.9 $N^{-1}$ at a larger force range of ~7 to 31 N (fig. S9). The U sensor showed similar linear sensitivity as the Octa sensor of ~2 $N^{-1}$ at a small force range of ~1 to 5 N and deteriorated to ~0.6 $N^{-1}$ only at a larger force range (fig. S10). The pressure sensor showed the highest linear sensitivity of 2.4 $N^{-1}$ to wide range of force from 1 to 31 N (fig. S11) compared to both strain sensors, offering the highest sensitivity for localized fetal kicking force detection. The temporal response of both Octa and pressure sensor was determined to be ~180 and ~140 ms (fig. S12), indicating the potential to determine rapid FM in principle, such as startles and twitches (*21*).

We further evaluated the Octa- and U-shaped sensors' response to strains applied in three directions (0°, 45°, and 90°) under varying strains of 5 to 30% at 1 Hz. The Octa sensor showed consistent electrical resistance change across all orientations under similar strains (fig. S13A), signifying isotropic omnidirectional sensitivity. In contrast, the U sensor exhibited anisotropic sensitivity, with maximum electrical resistance change observed vertically and horizontally, and minimal change at a 45° angle (fig. S13B). The sensitivity to strain is quantified as the gauge factor (GF) = $(\Delta R/R_0)/\epsilon$, where $\Delta R$ signifies the relative change in resistance, $R_0$ is the resistance of the sensor under no strain, and $\epsilon$ is the relative change in sensor length due to strain. The Octa sensor showed a stable GF across all tested angles (fig. S13C), further substantiating its high sensitivity omnidirectionally. However, the U sensor showed a decline in sensitivity at a 45° strain angle compared to its higher vertical and horizontal responses, demonstrating strain direction–dependent sensitivities.

Microscopic examination was used to examine the channel cracking patterns in the Octa and U sensors. Upon 0° vertical stretching, the average crack size in the Octa sensor increased by ~12.8% from ~16.5 to 29.3% as shown in fig. S14. Ninety-degree horizontal stretching led to widening of channel cracks from ~9.8 to ~26.3% (fig. S15), while 45° diagonal stretching expanded the channel cracks

by ~8.4% to an average of 24.9% (fig. S16). Such structural changes are in agreement with the omnidirectional sensitivities for the Octa sensor. In contrast, the U sensor has a broader initial crack area of ~29.7% and displayed variable crack expansion to 42.2% under horizontal strain, 38.6% vertical strain, and 36.1% at 45° strain (figs. S17 to S19), highlighting its unidirectional sensitivity to horizontal strains. Our results indicate that the change in the crack size was proportional to the GF for both Octa and U sensors (fig. S20).

### Detecting simulated fetal kicks in 3D abdomen skin

We next examined our sensors' capability in detecting fetal kicks in three-dimensional spaces. The setup included a force gauge, a 12-channel electrochemical workstation connected to a computer, and a rig with a silicone artificial abdomen 200 mm in internal diameter with 10 mm made of Ecoflex mounted on a homemade table (Fig. 2A). The artificial abdomen was parted into four major quadrants with additional three minor division in each major quadrants (fig. S21A), and four sensors were placed on each of the four outer quadrants of the artificial abdomen (fig. S21B).

A simulated kick force of ~15 N was applied to 57 well-defined locations inside the 3D dummy abdomen skin (fig. S21), in which four pressure sensors (Fig. 2B) and four Octa sensors (Fig. 2C) were conformally attached to the east, south, west, and north quadrants outside the dummy skin. The heat maps show that pressure sensors showed a more localized sensitivity, with each sensor covering about 4% of the abdomen area, monitoring up to 16% with all four (Fig. 2D). In contrast, the Octa sensor covered a broader area of ~23% per sensor, and the four Octa sensors together monitored over 90% of the artificial abdomen area (Fig. 2E).

In real-world scenarios, maternal movement could cause stray abdominal muscle strains that the Octa sensor might pick up. Therefore, a combination of one pressure sensor and one Octa sensor was tested by mounting them to the south and north quadrants of the 3D dummy skin (Fig. 2F). In this design, the Octa sensor offers wide sensitivity, and the pressure sensor provides localized detection. This configuration was chosen to leverage the complementary strengths of the two sensors: The Octa sensor provides broad omnidirectional strain detection but is susceptible to maternal movement artifacts, while the pressure sensor offers localized detection and is relatively insensitive to lateral muscle activity. We found that this combined pressure-strain sensing system could still detect ~50% of the artificial abdomen area (Fig. 2G).

We further examined our Octa sensors' ability to detect spatial loads by adjusting the force from 0.5 N to 4.5 N applied at a frequency of 1 Hz. As shown in fig. S22A, the Octa sensors in all four quadrants showed a similar change in electrical resistance when force is applied. Their normalized sensitivities were low when the force was applied at the center, and substantially high when loads were applied directly to them (fig. S22B).

Consistent with the corresponding 2D dummy skin, the Octa sensor was found to be advantageous for detecting omnidirectional strains in comparison to U sensors (fig. S23). On the same 3D dummy abdomen system in which both Octa- and U-shaped were mounted with 120° apart, 13 loads of ~15 N were applied at various angles (0°, 60°, 120°, and 180°) and surface distances (2, 4, 6, 10, and 12 cm) away from the sensors (fig. S23A). The Octa sensor displayed greater sensitivity than that of the U sensor as shown in the distance-dependent plot (fig. S23B) and the heatmap (fig. S23C).

We further developed a machine learning algorithm to detect the location and magnitude of simulated fetal kicks by using signals collected at 100 Hz, split into overlapping windows of varying sizes (1, 2, 3, and 5 s) with 50% overlap, and each window contained signals from all 4 sensors (fig. S24). Sixteen of 41 collected points were used as an independent test. For the remaining 25 points, 70% were used for training, 10% for validation, and 20% for testing. The moving mean and SD of the sensor were computed, and then $z$ score normalized the window by the statistics before the window. The performance of the location detection varied with the choice of the duration of the prior signals for normalization (table S1). Therefore, these normalized signals were then stacked into a one-dimensional vector, and a six-layer multilayer perceptron (MLP) was used to detect the longitude, latitude, and force magnitude of the movement (fig. S24C). A six-layer MLP was trained and tested using $z$ score normalized signals to predict longitude, latitude, and force magnitude, with haversine distance used to measure location accuracy on the hemisphere-shaped artificial abdomen. The stacked model with a 1-s window size performed best for "seen" locations, achieving a mean distance of 1.2 mm and a force mean absolute error (MAE) of 0.13 N (Fig. 2H). However, for "unseen" locations, the accuracy decreased with a mean distance of 26.5 mm, although force detection remained reliable with an MAE of 0.44 N (Fig. 2I), suggesting increased data points could improve generalizability.

### Lightweight, compact wearable FM patch

To demonstrate the clinical utility of the Octa sensor and pressure sensor for detecting FM, we developed two soft, thin, and flexible wearable patches incorporating one Octa and one pressure sensor. These devices were designed to conform to the abdomen of pregnant patients, are shown in Fig. 3A. The exploded view (Fig. 3, B and C) highlights the patches' construction, featuring a soft polyimide (PI)–based flexible printed circuit (FPC) that integrates a thin lithium polymer battery and electronic integrated circuit chips, all encapsulated with kinesiology tape, which is then adhered to the patient's abdomen using a medical double-sided silicone adhesive.

The Octa sensor is attached to a separate PI-based FPC connector, which allows easy replacement after each study (Fig. 3B). In contrast, the pressure sensor (Fig. 3C) is mounted on the double-sided silicone adhesive, contacting the interdigitated electrode beneath the primary device. The adhesive was replaced after each trial for hygiene purposes, also replacing the pressure sensor with a fresh sensor. The Octa and pressure sensor patches are lightweight and compact, measuring 63 mm by 30 mm by 4 mm (Fig. 3D) and 62 mm by 28 mm by 2 mm (Fig. 3E), respectively. As the human abdomen has a curvilinear surface, we designed the patch to provide multiple bendable locations so that the device can be bent (Fig. 3F) to conform to the curvature of the patient's abdomen. At the same time, stiffeners will provide additional support to the rigid electronic chips to prevent bending that leads to delamination of chips from the copper trace on the FPC (fig. S25).

The functional diagram in Fig. 3G outlines the device architecture, with red arrows indicating power supply and blue arrows representing data flow. Each device features a lithium battery, a voltage-regulating circuit, a sensor with a signal conditioning circuit, and a Bluetooth radio frequency system on a chip for reading the sensor's electrical resistance, storing data on a MicroSD card, and communicating with a smartphone app.

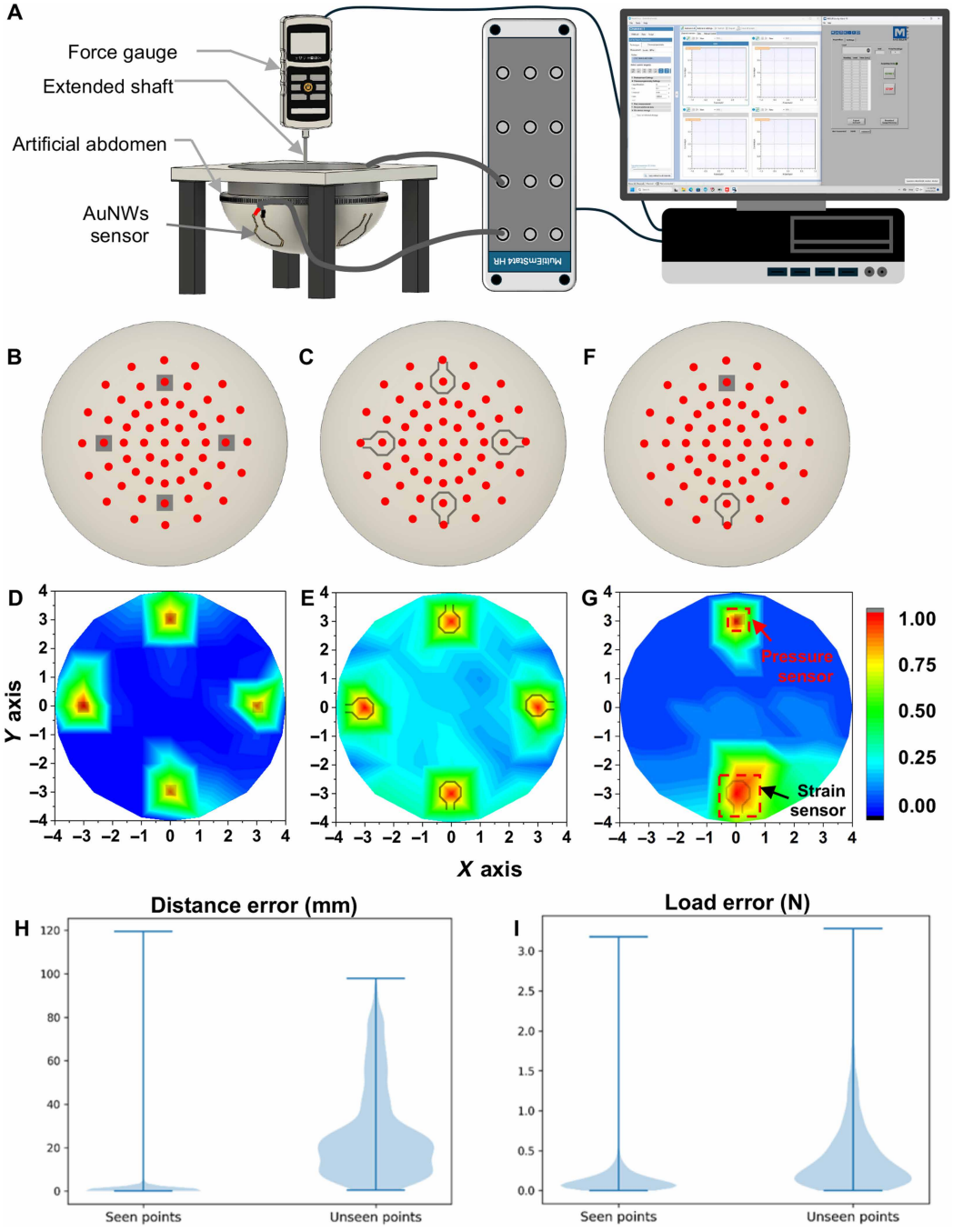


**Fig. 2. Simulated FMs in a 3-dimensional artificial abdomen system.** (**A**) Schematic illustration of 3D fetal simulator setup; Illustration of the force application points corresponding to the location of (**B**) four pressure sensors, (**C**) four Octa sensors, and (**D**) one pressure sensor and one Octa sensor mounted on 3D FM simulator. Heatmap plot of the sensitivities of the (**E**) four pressure sensors, (**F**) four Octa sensors, and (**G**) one pressure sensor and one Octa sensor to load applied. (**H**) The distribution of the distance and the load's MAE of testing seen points and (**I**) unseen points from the best model for the detection of simulated FMs.

## Clinical studies

The lightweight, compact, and Band-Aid–like patch offered a user-friendly form factor, enabling a straightforward stick-and-play application for real-world use with pregnant patients. We conducted trials on 59 pregnant women positioned semi-recumbently. The pressure sensors were attached to the area of the abdomen where the most vigorous FMs were felt by the mother, typically in the lower quadrant (Fig. 4A). The strain sensor was typically attached to the quadrant closest to fetal limbs. An accelerometer was added and placed on the participant's chest. This accelerometer was used to capture non-FM data for signal denoising and training the machine learning model and is not intended to be part of the final wearable pressure-strain combo for FM monitoring.

The small footprint size enabled a simultaneous validation study against ultrasound imaging. A trained sonographer performed the ultrasound scan and annotated various FM on the recorded

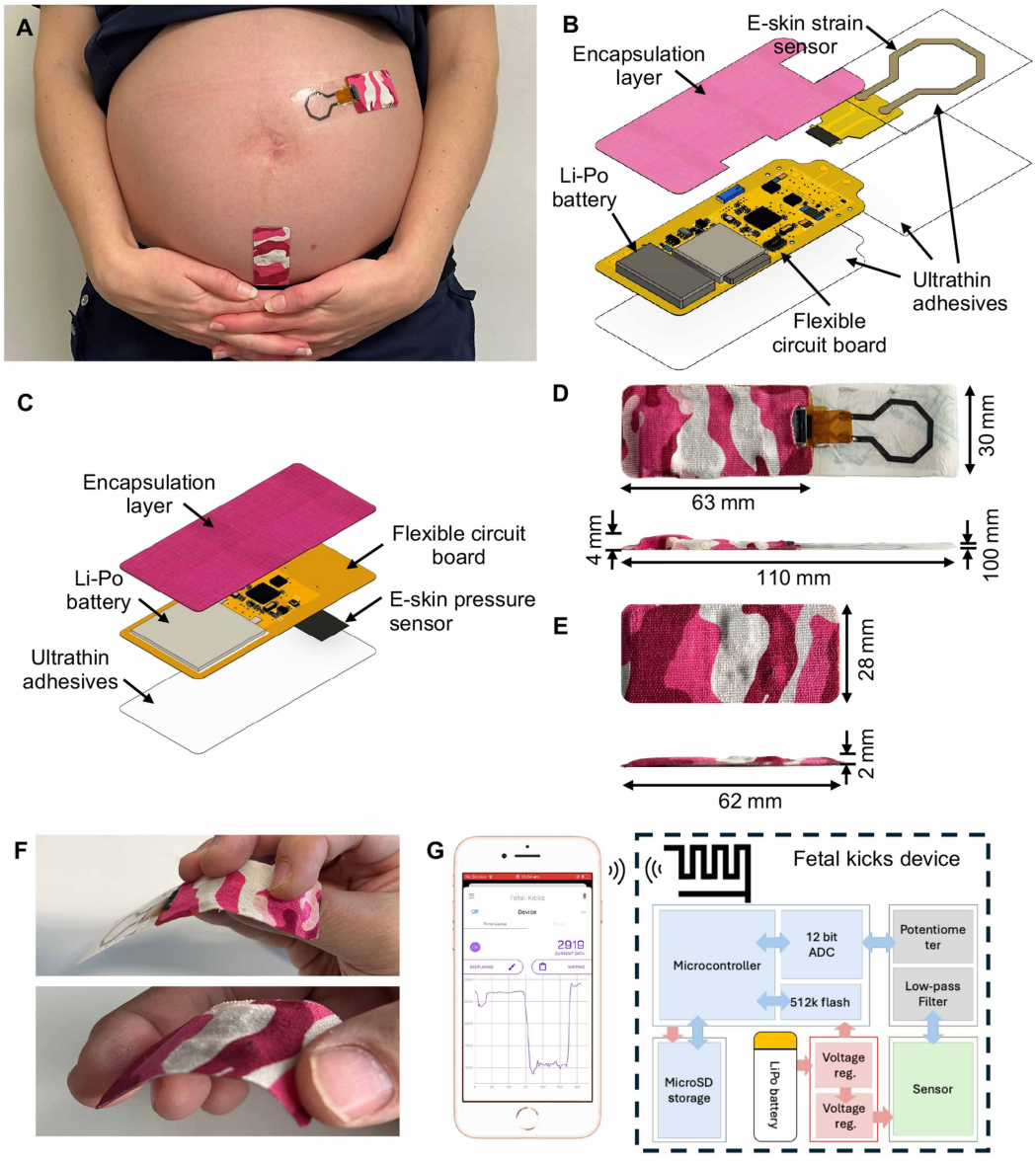


**Fig. 3. Pressure and strain combo sensor system.** (**A**) Photograph of the fetal kicks strain sensor and pressure sensor device on a pregnant mother. Exploded illustration of the fetal kicks (**B**) strain sensor and (**C**) pressure sensor device; dimension of the fetal kicks (**D**) strain sensor and (**E**) pressure sensor device. (**F**) Photograph of the fetal kicks strain sensor and pressure sensor device being flexed and (**G**) electronic schematic of the fetal kicks devices.

ultrasound video (Fig. 4B), including trunk movement, kicking, breathing, twitching, head movements, startle, waving, hiccups, and fetal behavioral state. Figure 4C displays a particular truncated plot set comprising synchronized time series signals from pressure and Octa sensors along with a three-axis chest accelerometer. It shows that the pressure patch could well detect localized FM events of breathing, twitching, and kicking, whereas the strain patch could detect nonlocalized signals like kicking movements. The accelerometer signals were generally featureless, except during instances of ultrasound probe movement or conversations. In another dataset, we found that both pressure and strain patches could detect fetal trunk movement and kicking with a similar magnitude (fig. S26, A and B). The strain sensor achieved better sensitivity than the pressure patches in identifying nonlocalized FM, including hiccups, head motions, and fetal behavioral states (fig. S26, C to E). Fetal behavioral state (fBS) refers to distinct patterns of fetal activity and rest, reflecting the health of the fetal central nervous system (*22*). Such movements, while potentially straining the participant's abdomen, may not always align perpendicularly to pressure sensors, influencing movement detections. On the other hand, fetal twitching, startle, and waving movements were well detected by the pressure sensor but not the strain sensor (fig. S26, G to I). Twitching, waving and startling are movements that happen in a sudden split second (*23*), which could cause a spike in perpendicular loads applied to the pressure patches directly. Such motion caused minute lateral MAS straining; hence, the strain sensor recorded featureless background signals.

Despite these encouraging results, we also observed the interferences from ultrasound probe movements, participants' random

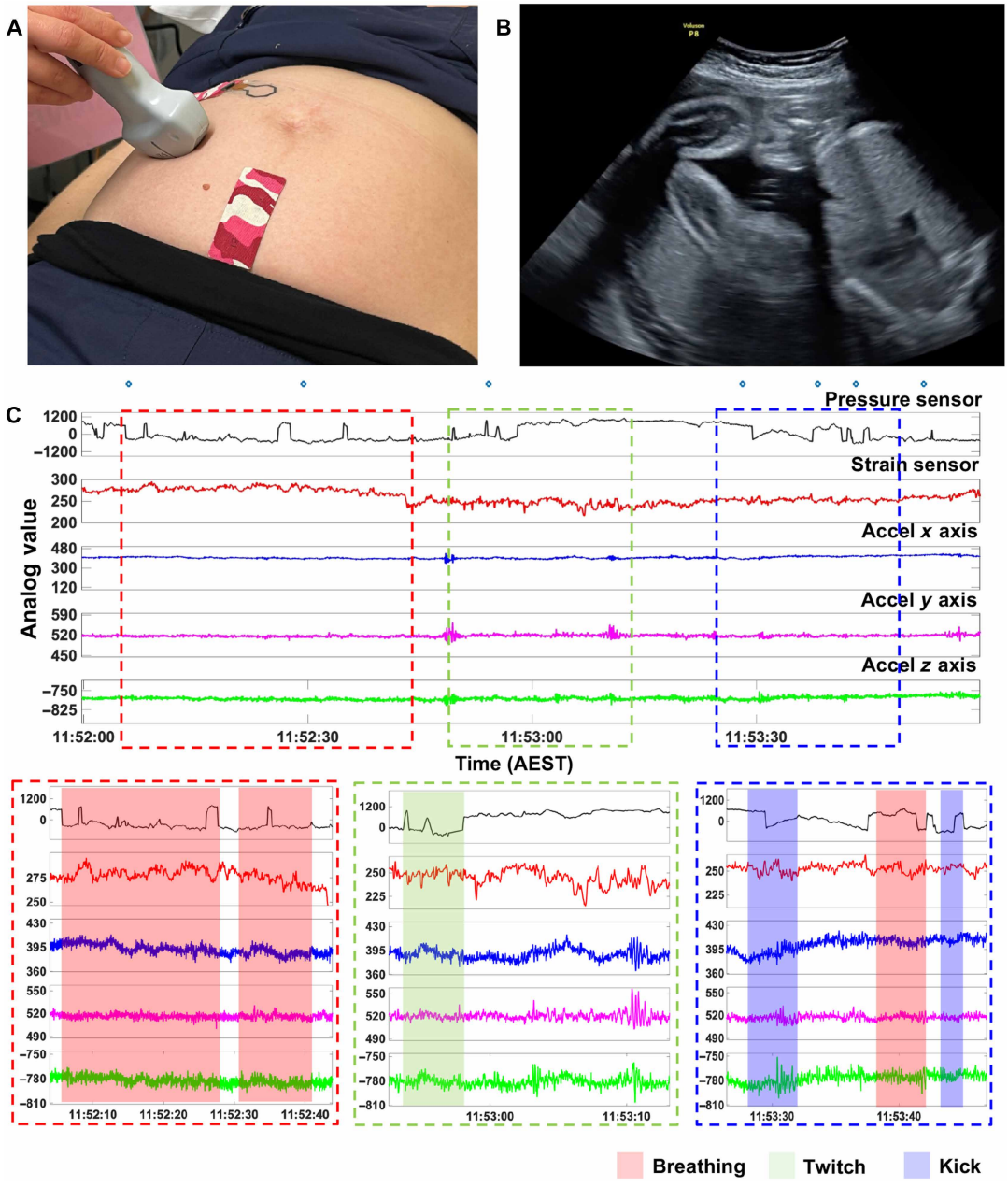


**Fig. 4. Multimodal signal recordings.** (**A**) Photographic image of the fetal kicks device on a clinical trial volunteer while undergoing an ultrasound scan. (**B**) Snapshot image of the ultrasound video recording. (**C**) Representative signal from pressure sensor, strain sensor, and accelerometer during trial.

motions such as speaking or body movements, which we could not label. To take account of these complex real-world scenarios, we further developed a machine learning algorithm designed to distinguish between FM and non-FM detections in a binary classification setting. The algorithm's ability to detect the presence of FM within 4-s time windows was evaluated using the area under the receiver operating characteristic (AUROC). The raw data from pressure and strain sensors were preprocessed according to the flow diagram shown in fig. S27A.

The performance of the pre- and post-denoised Octa and pressure sensor signal using accelerometer-detected maternal movements was evaluated. Figure S28A showed denoised Octa sensor signal improved the AUROC by 14.87%, whereas the denoised pressure sensor signal resulted in a 1.52% reduction in AUROC, suggesting over-denoising and potential loss of critical features.

We further compared the performance of single-sensor systems and the pressure-strain combined system. For the single-sensor system, the pressure sensor achieved an AUROC of 89.51%, while the Octa sensor achieved an AUROC of 84.55% (Fig. 5A). The combo system was developed by integrating results from both sensors, where 24 of 59 participants were equipped with both Octa and pressure sensors, which yielded best AUROC of 92.18% (Fig. 5B).

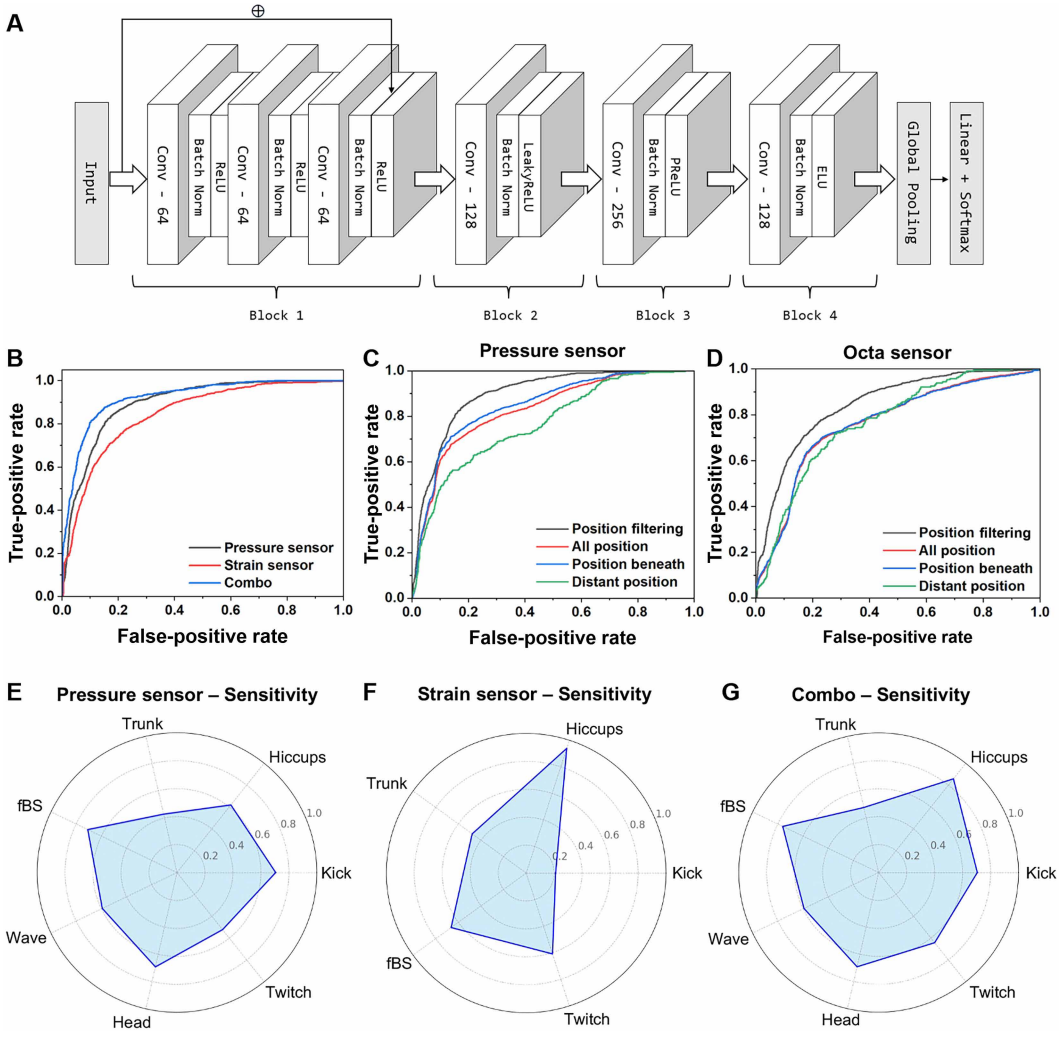


**Fig. 5. Machine learning of pressure and strain combo sensor system.** (**A**) Model architecture of ResCNN. It includes CNN for feature extraction, batch normalization to enhance learning stability, and uses a residual learning block with a shortcut connection in the first three convolutional layers to capture complex patterns. (**B**) Area under receiver operating characteristic curve for strain sensor (black), pressure sensor (red), and combo sensor (blue) in comparison with random guesses. Impact analysis of relative position filtering on the performance of (**C**) pressure sensor and (**D**) Octa sensor. "All position" refers to all samples without filtering, "position beneath" refers to samples located directly beneath the sensor, and "distant position" refers to samples located farther away from the sensor. Sensitivity radar chart for (**E**) pressure sensor, (**F**) strain, and (**G**) combo sensor when detecting FM.

Additional performance metrics, such as sensitivity, specificity, and F1 score, are presented in figs. S28 to S31. Specifically, the combined system achieved a sensitivity of 78.16% and a specificity of 90.86%.

The impact of relative position filtering on model performance shows pressure sensor could achieve a detection accuracy of AUROC 84.65% for FM directly beneath it, compared to 76.70% for those farther away, indicating greater sensitivity to localized FM (Fig. 5C). The Octa sensor, however, showed <0.5% performance difference between samples at different distances, suggesting minimal effect to positional variations (Fig. 5D). Other factors, such as body mass index (BMI), amniotic fluid index, and the device distance to the fetus, showed minimal statistical significance (fig. S32 and table S3), indicating the capability of the sensors to function effectively across diverse conditions.

Post hoc analysis of detection results for different FM subcategories was performed on the validation set, where pressure sensor exhibited more balanced sensitivity across different FM including head movements, hiccups, kicks, twitches, waves, trunk movements, and fBS (Fig. 5E). Because of limited dataset after relative position filtering, the Octa sensors showed effective detection of fetal hiccups but lower sensitivity for twitches, trunk movements, kicks, and fBS (Fig. 5F). The combination of Octa and pressure sensor showed ability to effectively compensate each other's shortcomings, leading to improved overall sensitivity in detecting hiccups, trunk movements and fBS, while preserving the sensitivity to other types of FM (Fig. 5G). This showed that our system has the potential to detect individual FM types if the external noise factors such as maternal movements and environmental noise, can be eliminated.

In ambulatory or home-use settings, temperature and humidity may influence sensor performance. To assess the environmental robustness of our sensors, both Octa and pressure sensors were tested under varying conditions by applying cyclical forces ranging from 0

to 30 N at different temperatures (14°, 23°, and 37°C) and relative humidity levels (53, 75, and 92%). Both Octa and pressure sensors exhibited stable and closely overlapping $\Delta R/R_0$ response curves across all test conditions as shown in fig. S33, indicating minimal hysteresis variation and strong environmental tolerance.

To assess the long-term operational performance of the fetal kicks system, both Octa sensor and pressure sensor were tested on a nongravid participant. As shown in fig. S34, both sensors maintained stable signal acquisition, with no substantial signal degradation, while the battery voltage gradually declined from ~4.2 to ~3.5 V over 25 hours. These results demonstrate that the system is capable of continuous operation over a full day on a single charge. To evaluate mechanical durability, both the Octa strain sensor and pressure sensor were tested with 1000 cyclic loads of ~30 N followed by an additional 10 postfatigue cycles. As shown in figs. S35 and S36, both sensors demonstrated stable, repeatable responses with negligible signal degradation, confirming their long-term stability.

## DISCUSSION

FM monitoring technologies are essential for assessing fetal health, enabling early detection of potential complications, and improving pregnancy outcomes. Current methods primarily rely on ultrasound imaging, Doppler technology to detect motion-induced frequency shifts, and emerging wearable IMU sensors that measure linear acceleration and angular velocity. However, these technologies often suffer from bulkiness, inconvenient usage, large footprint sizes, dependency on a skilled workforce to interpret the results, and susceptibility to complex interferences. As such, they are typically used intermittently and only in high-risk populations, likely the explanation for their limited impact on reducing the rate of stillbirth.

We proposed an approach that offers the prospect of continuous FM surveillance suitable for use in all pregnant women. Our design concept utilizes soft, conformal, lightweight wearable force-sensing Band-Aids to directly detect deformations of the maternal abdominal skin, which are indirectly related to FM.

With this design concept in mind, we developed an AI-powered, compact wearable pressure-strain combo sensor system allowing continuous FM monitoring. In this combo system, the wearable Octa strain sensor featured isotropic omnidirectional sensitivity, enabling detection of maternal abdominal over a large area, whereas, the wearable pressure sensor offered high sensitivity with a small domain, advantageous for accurate localized FM detection. In the 2D simulated artificial MAS, the Octa sensor could detect omnidirectional strains up to an area of ~76.8 $cm^2$; the pressure sensor was only highly sensitive to localized strain, covering only ~12.6 $cm^2$, offering benefit to pinpoint the precise location of the FM. Similarly, in a 3D artificial MAS system, the Octa sensor demonstrated broader sensitivity, making it suitable for applications requiring a wider sensing area; the pressure sensor exhibited localized pressure sensitivity, highlighting its capacity to deliver precise measurements in targeted areas.

Integrating the two soft, flexible Octa and pressure sensors into wearable Band-Aids, our system was able to detect up to nine types of FM, including trunk movement, kicking, breathing, twitching, head movements, startle, waving, hiccups, and fBS. With residual convolutional neural network (ResCNN) machine learning techniques for preclinical trial data analysis, the pressure sensor achieved an impressive AUROC accuracy of 89.51% in detecting FM, while the Octa sensor reached an AUROC of 84.55%. Notably, the pressure sensor demonstrated higher sensitivity for movements directly beneath it compared to those farther away, whereas the Octa sensor maintained consistent performance across different distances, showcasing its reliability and wider sensing area. The combination of both sensor types resulted in a substantial performance enhancement, yielding an overall AUROC accuracy of 92.18% in binary detection of FM, illustrating the potential of combining diverse sensing modalities to achieve more accurate and reliable monitoring outcomes. Our wearable force-sensing Band-Aid–based fetal monitoring solution shows outstanding capability to distinguish binary FM and non-FM with high accuracy, and potentially identify different types of FM, paving the way for advanced continuous and user-friendly ambulatory continuous FM monitoring.

Since the 1970s, studies that have explored FM counting as an approach to fetal wellbeing assessment (*24*) have relied on maternal perception (*25*), requiring mothers to record the frequency and intensity of FM over time (*26*). However, mothers perceive only a portion of actual FM (*23*), likely explaining why maternal FM counting has not proven effective in reducing stillbirth (*5*, *27*, *28*). Our wearable technology introduces a new strategy for continuous, non-invasive, and objective measurement of FM. Future large-scale clinical studies in out-of-hospital real-world settings are needed to evaluate fetal kicks and investigate the relationship between FM patterns and pregnancy complications. If validated, this technology could offer pregnant women greater reassurance about fetal health and wellbeing.

## MATERIALS AND METHODS

### Materials

The following materials were obtained from Sigma-Aldrich: gold (III) chloride trihydrate, 4-mercaptobenzoic acid, (3-aminopropyl) triethoxysilane, sodium borohydride, sodium citrate tribasic dihydrate (99.0%), L-ascorbic acid, and polystyrene-block-poly(ethylene-ran-butylene)-block-polystyrene, along with liquid metal (eutectic gallium-indium). Toluene was sourced from MERCK, and absolute ethanol from Ajax Finechem. Ecoflex 00-30 and Dragon Skin were acquired from Smooth-On Inc. The bare silicon wafer was purchased from Electronics and Materials Corporation. All solutions were prepared using Millipore Milli-Q water (resistivity >18 megohm $cm^{-1}$). All chemicals were used as received unless otherwise indicated.

### Methods

#### *Fabrication of AuNWs/SEBS strain sensor*

The AuNWs were fabricated on the basis of a modified seed-mediated approach. First, 2-nm gold seeds were synthesized by mixing 0.25 ml of $25 \times 10^{-3}$ M gold (III) chloride trihydrate and 0.147 ml of $3.4 \times 10^{-2}$ M sodium citrate in a conical flask with 20 ml of $H_2O$ under vigorous stirring; 1 min later, 600 μl of ice-cold 0.1 M $NaBH_4$ solution was added to the solution, which was stirred for 5 min until the color turned from light yellow to red. The gold seed solution was stored in the fridge at 4°C until needed. To fabricate the thin film strain sensor, a thin SEBS layer (0.15 g/ml in toluene) was first spin-coated onto a bare silicon wafer at 500 RPM for 1 min, then cured in an oven at 60°C for 5 min. The SEBS-coated wafer was then surface-treated with oxygen plasma for 5 min to prepare for AuNWs strain sensor growth. Next, the silicon wafer was immersed in a $5 \times 10^{-3}$ M solution of (3-aminopropyl)triethoxysilane in ethanol for 1 hour to functionalize the surface with amino groups. After rinsing twice

with ethanol, the amino-functionalized SEBS was immersed in a citrate-stabilized gold seed solution for 1 hour, followed by two water rinses to remove excess seed particles. A photomask with the cutout of Octa and U sensor was prepared using glossy vinyl sticker cut using the Silhouette Cameo 4 vinyl cutter and stick onto the surface of SEBS. The silicon wafer was then immersed in a growth solution containing $9.8 \times 10^{-4}$ M 4-mercaptobenzoic acid, $1.2 \times 10^{-2}$ M gold (III) chloride trihydrate, and $2.9 \times 10^{-2}$ M L-ascorbic acid for 1 to 5 min, resulting in the formation of AuNWs thin films with the shape of Octa and U sensor. After the AuNWs grow, the mask is peeled off on a hot plate (50° to 55°C) using tweezers with a few drops of ethanol applied at opening between the photomask and SEBS. After confirming the resistance range of each sensor, which ranges between 200 to 500 ohms, the sensors are transferred from the wafer to a release liner using a polyvinyl alcohol (PVA) tape. The PI extensor that connects to the fetal kicks device was assembled to the SEBS with ProTac acrylic adhesive, and the connection was reinforced with the liquid metal (eutectic gallium-indium). The sensor was then sealed by applying a thin layer of Dragon Skin FX Pro on the top and bottom of the strain sensor. Last, the sealed sensor was sandwiched between two Tegaderm 1622 W dressings.

### Sensor characterization

SEM images were characterized using a FEI Nova NanoSEM 450 FEGSEM operated at 5 kV beam voltage. A Nikon SMZ800 microscope took optical images with a Nikon Digital Sight DS-Fi1 camera. The 2D strains to the AuNWs grown SEBS were measured by a linear translation stage with an integrated controller and stepper motor (ThorLabs LTS150/M). The 3D strains were tested on the DT using a MARK-10 (series 7) force gauge mounted on a test stand ESM301. The current differences and the *I*-*V* characteristics for the pressure sensor were recorded by the Parstat 4000A electrochemical system (Princeton Applied Research). To test the electrical-pressure responses, the samples are attached onto a lab-developed test stand (ThorLabs LTS150/M in vertical setting with a Mark-10 Series 7-20 force gauge). The probe from the force gauge was lowered from the top onto the sensor to provide a pressure. The speed was controlled by the Thorlabs linear stage.

### Finite element analysis

The FEA was carried out using Autodesk Simulation. The elastic modulus ($E$) and Poisson's ratio ($\nu$) are $E_{\text{silicone}} = 0.3$ GPa and $\nu_{\text{substrate}} = 0.49$ for the simulated maternal and $E_{\text{Au}} = 82.7$ GPa and $\nu_{\text{Au}} = 0.42$ for simulated gold nanowires Octa and U sensor.

### Data collection

In the clinical trials, sensor data were collected from 59 pregnant women. Among them, 32 wore chest accelerometers between 28 and 37 weeks of gestation. Pressure sensor signals were collected from 51 women, each of whom wore one pressure sensor, with 31 of these women also having accelerometer data. Octa sensor signals were collected from 48 women, each wearing one to three Octa sensors at different positions, leading to a total of 77 sensor data files. Of these women, 27 also had accelerometer data, corresponding to 41 sensor files. The participants had a BMI ranging from 23 to 46. All participants were carrying singleton pregnancies with no reported complications, fetal anomalies, or comorbidities at the time of participation. Fetal kicks and other movements were visually identified and annotated in real time by trained sonographers using ultrasound scans. The ultrasound video and the sensor signals were recorded in parallel, and time-synchronized annotations were used as ground truth for FM detection model training and evaluation.

### Data processing

Signal preprocessing consists of seven main steps. First, an 8th-order Butterworth low-pass digital filter with a cutoff frequency of 8 Hz was applied to the sensor data. The signal was resampled to achieve a consistent sampling rate of 50 Hz. For the Octa sensor, principal components analysis (PCA), an unsupervised machine learning algorithm, was used to reduce the three-dimensional chest accelerometer data to a single dimension. PCA was chosen to reduce redundancy and retain the most informative component of the accelerometer data. This resulting signal was used to eliminate maternal movement noise from the Octa sensor data via spectral subtraction. The original pressure sensor signal was retained, as denoising resulted in critical information loss during ablation studies (refer to fig. S28A for the ablation study of the denoising method). Fetal breathing was excluded as they are intermittent (*24*) and not all fetal breathings were observed in ultrasound scans and annotated. Relative position filtering was applied, assuming that sensors could only detect FM related to the sensor's relative position to the fetus. For instance, a sensor placed on the fetus's feet was expected to detect kicking and twitching, but not head movements. As a result of this filtering process, the number of clinician-annotated signal-FM pairs was reduced from 1833 to 1250. Similar to the signal processing step in the simulation experiment, moving average normalization was then applied, using the mean and SD calculated over the preceding 1, 3, and 5 s, respectively. The normalized results were concatenated into three-dimensional data. Last, the signal data were segmented using a fixed window of 4 s, and a balanced binary dataset of movement and nonmovement samples was constructed through down-sampling.

### Machine learning analysis

We compared different machine learning algorithms, including the linear models such as logistic regression (LR), the nonlinear model decision tree (DT), and nonlinear models like neural network models, including MLP, bidirectional long short-term memory, and ResCNN as shown in fig. S29. We implemented L2-regularized LR and DT models with Gini impurity criterion for node splitting using Python's scikit-learn library. All neural network models were implemented using PyTorch, using the Adam optimizer along with an automatic learning rate search method. The binary cross-entropy loss function was used during training. The batch size was set to 128 and the maximum number of epochs was set to 30, with the model achieving the highest AUROC on the validation set selected as the best model. The experiment followed a leave-one-subject-out cross-validation setup, with separate models trained for each sensor type. We developed a two-sensor system, where a weighted sum of detection probabilities from the two sensors was used to improve detection accuracy. For all participants, a unified weighting coefficient was searched. In addition, a case-by-case study was performed to search for the optimal weighting coefficients for each individual to analyze the weight distribution.

### Clinical testing

The research protocol was approved by Monash Health's Human Research Ethics Committee (RES-17-0000-028) and registered on the Australian New Zealand Clinical Trials Registry (ACTRN1261700-0410358). Participants were recruited via convenience sampling from women presenting to the Day Assessment Unit at Monash Health for evaluation of reduced FMs. Participants were included in the study if they were aged over 18 years, had a singleton pregnancy, were at least 28 weeks' gestation, and were aware of normal FM on

the day of the ultrasound. Participants were excluded if they had any intellectual or mental impairment, allergies to latex or Elastoplast, known fetal congenital abnormalities, preexisting relationships with the fetal kicks research team, were highly dependent on medical care, or had a body weight exceeding 200 kg. If participants are eligible, an informed consent will be obtained before participating the trial. Participants will be in a semi-recumbent position while an ultrasound is carried out by a trained sonographer or clinician for a duration of 20 min. During this time, the fetal kicks devices will be worn by the patient. The trained sonographer will observe FM (gross movement of trunk and isolated limb movement) and annotate the time and types of movement visualized.

## Supplementary Materials

**This PDF file includes:**

Supplementary Text
Figs. S1 to S36
Tables S1 to S3

## REFERENCES AND NOTES


1. S. Neldam, Fetal movements as an indicator of fetal wellbeing. *Lancet* **315**, 1222–1224 (1980).
2. F. Sergent, A. Lefevre, E. Verspyck, L. Marpeau, Decreased fetal movements in the third trimester: What to do? *Gynecol. Obstet. Fertil.* **33**, 861–869 (2005).
3. S. Preston, K. Mahomed, Y. Chadha, V. Flenady, G. Gardener, J. MacPhail, L. Conway, L. Koopmans, T. Stacey, A. Heazell, R. Fretts, F. Frøen, "Clinical practice guideline for the management of women who report decreased fetal movements," (The Australia and New Zealand Stillbirth Alliance (ANZSA), 2010).
4. L. M. Daly, G. Gardener, V. Bowring, W. Burton, Y. Chadha, D. Ellwood, F. Froen, A. Gordon, A. Heazell, K. Mahomed, S. McDonald, J. E. Norman, J. Oats, V. Flenady, Care of pregnant women with decreased fetal movements: Update of a clinical practice guideline for Australia and New Zealand. *Aust. N. Z. J. Obstet. Gynaecol.* **58**, 463–468 (2018).
5. L. Mangesi, G. J. Hofmeyr, V. Smith, R. M. Smyth, Fetal movement counting for assessment of fetal wellbeing. *Cochrane Database Syst. Rev.* **2015**, CD004909 (2015).
6. A. K. Ghosh, D. S. Catelli, S. Wilson, N. C. Nowlan, R. Vaidyanathan, Multi-modal detection of fetal movements using a wearable monitor. *Inform. Fusion* **103**, 102124 (2024).
7. A. K. Ghosh, O.-I. Shahid, N. C. Nowlan, R. Vaidyanathan, Comparative performance evaluation of fetal movement-detecting wearable sensors using a body-worn device. *IEEE Sens. J* **24**, 28018–28027 (2024).
8. T. Ouypornkochagorn, W. Dankul, L. Ratanasathien, Fetal movement detection with a wearable acoustic device. *IEEE Sens. J* **23**, 29357–29365 (2023).
9. J. Lai, R. Woodward, Y. Alexandrov, Q. A. Munnee, C. C. Lees, R. Vaidyanathan, N. C. Nowlan, Performance of a wearable acoustic system for fetal movement discrimination. *PLOS ONE* **13**, e0195728 (2018).
10. J. Y. Xu, C. Zhao, B. Ding, X. X. Gu, W. R. Zeng, L. Qiu, H. Yu, Y. Shen, H. Liu, Fetal movement detection by wearable accelerometer duo based on machine learning. *IEEE Sens. J* **22**, 11526–11534 (2022).
11. Y. C. Du, L. B. Yen, P. L. Kuo, P. Y. Tsai, A wearable device for evaluation of relative position, force, and duration of fetal movement for pregnant woman care. *IEEE Sens. J* **21**, 19341–19350 (2021).
12. M. Altini, P. Mullan, M. Rooijakkers, S. Gradl, J. Penders, N. Geusens, L. Grieten, B. Eskofier, Detection of fetal kicks using body-worn accelerometers during pregnancy: Trade-offs between sensors number and positioning. *Annu. Int. Conf. IEEE Eng. Med. Biol. Soc.* **2016**, 5319–5322 (2016).
13. A. Jimenez-Gonzalez, C. J. James, Time-structure based reconstruction of physiological independent sources extracted from noisy abdominal phonograms. *I.E.E.E. Trans. Biomed. Eng.* **57**, 2322–2330 (2010).
14. S. W. Verbruggen, B. Kainz, S. C. Shelmerdine, J. V. Hajnal, M. A. Rutherford, O. J. Arthurs, A. T. M. Phillips, N. C. Nowlan, Stresses and strains on the human fetal skeleton during development. *J. R. Soc. Interface* **15**, 20170593 (2018).
15. X. Zhao, X. Zeng, L. Koehl, G. Tartare, J. De Jonckheere, A wearable system for in-home and long-term assessment of fetal movement. *IRBM* **41**, 205–211 (2020).
16. S. Layeghy, G. Azemi, P. Colditz, B. Boashash, Non-invasivemonitoring of fetal movements using time-frequency features of accelerometry, in *IEEE International Conference on Acoustics, Speech and Signal Processing (ICASSp 2014), Florence, Italy, 2014* (United States, Institute of Electrical and Electronics Engineers, Piscataway, NJ, 2014).
17. Y. O. Bobrova, Y. A. Zhivolupova, Automatic detection of abnormal fetal states by means of a personal monitoring system, *Proceedings of 2017 Xx Ieee International Conference on Soft Computing and Measurements (Scm)* (2017), pp. 782–784.
18. Y. Wang, S. Gong, D. Gomez, Y. Ling, L. W. Yap, G. P. Simon, W. Cheng, Unconventional janus properties of enokitake-like gold nanowire films. *ACS Nano* **12**, 8717–8722 (2018).
19. Y. Wang, S. Gong, S. J. Wang, X. Y. Yang, Y. Z. Ling, L. W. Yap, D. S. Dong, G. P. Simon, W. L. Cheng, Standing Enokitake-like nanowire films for highly stretchable elastronics. *ACS Nano* **12**, 9742–9749 (2018).
20. S. Gong, L. W. Yap, B. Zhu, Q. Zhai, Y. Liu, Q. Lyu, K. Wang, M. Yang, Y. Ling, D. T. H. Lai, F. Marzbanrad, W. Cheng, Local crack-programmed gold nanowire electronic skin tattoos for in-plane multisensor integration. *Adv. Mater.* **31**, e1903789 (2019).
21. J. I. de Vries, G. H. Visser, H. F. Prechtl, The emergence of fetal behaviour. I. Qualitative aspects. *Early Hum. Dev.* **7**, 301–322 (1982).
22. J. G. Nijhuis, H. F. Prechtl, C. B. Martin Jr., R. S. Bots, Are there behavioural states in the human fetus? *Early Hum. Dev.* **6**, 177–195 (1982).
23. J. I. de Vries, B. F. Fong, Normal fetal motility: An overview. *Ultrasound Obstet. Gynecol.* **27**, 701–711 (2006).
24. A. Burgess, M. Aucutt, S. L. Coleman, Standardizing fetal movement monitoring using count the kicks. *MCN Am. J. Matern. Child Nurs.* **49**, 306–313 (2024).
25. S. Patel, A. E. Conway, T. Adjei, I. Abati, S. Dhawan, Z. Yu, R. Vaidyanathan, C. Lees, Is it possible to monitor fetal movements with a wearable device? A review of novel technologies. *Eur. J. Obstet. Gynecol. Reprod. Biol.* **305**, 329–338 (2025).
26. J. F. Froen, A kick from within–fetal movement counting and the cancelled progress in antenatal care. *J. Perinat. Med.* **32**, 13–24 (2004).
27. A. Grant, D. Elbourne, L. Valentin, S. Alexander, Routine formal fetal movement counting and risk of antepartum late death in normally formed singletons. *Lancet* **334**, 345–349 (1989).
28. F. Bellussi, G. Po, A. Livi, G. Saccone, V. De Vivo, E. A. Oliver, V. Berghella, Fetal movement counting and perinatal mortality: A systematic review and meta-analysis. *Obstet. Gynecol.* **135**, 453–462 (2020).


**Acknowledgments:** This work was performed in part at the Melbourne Centre for Nanofabrication (MCN) in the Victorian Node of the Australian National Fabrication Facility (ANFF). We acknowledge the facilities and the scientific and technical assistance of the Research and Prototype Foundry Core Research Facility at the University of Sydney, part of the NSW node of the NCRIS-enabled Australian National Fabrication Facility. We also acknowledge the use of facilities within the Monash Centre for Electron Microscopy (MCEM). We acknowledge the technical and scientific assistance of Sydney Microscopy & Microanalysis, the University of Sydney node of Microscopy Australia. **Funding:** This work was supported by the National Health and Medical Research Council Ideas Grant (2004444, L.W.Y., V.S., J.M.M., F.M., and W.C.), National Health and Medical Research Council Investigator Grant (2010154, W.C.), Jack Brockhoff Foundation (4659-2019, S.G.), National Health and Medical Research Council (MRF2028865, A.L.J.), National Heart Foundation of Australia (105863, A.L.J.), National Heart Foundation of Australia (106979, A.L.J.), and Snow Medical (2022SF176, A.L.J.). **Author contributions:** Conceptualization: L.W.Y., A.L., D.N., D.V.A., V.S., J.M.M., B.W.M., E.M.W., Z.G., F.M., and W.C. Methodology: L.W.Y., A.L., Y.J., D.N., S.G., X.Z., T.I., V.S., A.T., A.W., J.L., J.M.M., B.W.M., E.M.W., Z.G., F.M., and W.C. Investigation: L.W.Y., A.L., Y.J., D.N., S.G., R.W., D.V.A., Y.L., V.S., A.T., A.W., Y.Z., J.L., E.M.W., and F.M. Resources: L.W.Y., D.N., S.G., Y.L., V.S., A.T., A.W., J.M.M., E.M.W., A.L.J., Z.G., and F.M. Data curation: L.W.Y., A.L., Y.J., D.N., S.G., D.V.A., V.S., A.T., and F.M. Validation: L.W.Y., A.L., Y.J., D.N., S.G., Y.L., T.I., A.T., and F.M. Formal analysis: L.W.Y., A.L., Y.J., D.N., S.G., D.V.A., Q.L., Y.L., R.G., X.Z., T.I., V.S., A.W., E.M.W., and A.L.J. Funding acquisition: L.W.Y., V.S., J.M.M., E.M.W., A.L.J., F.M., and W.C. Supervision: L.W.Y., D.N., J.M.M., B.W.M., E.M.W., A.L.J., Z.G., F.M., and W.C. Software: L.W.Y., Y.J., D.N., D.V.A., R.G., X.Z., T.I., V.S., A.L.J., Z.G., and F.M. Visualization: L.W.Y., A.L., Y.J., D.N., R.G., T.I., A.T., J.L., S.A.M., A.L.J., and F.M. Project administration: L.W.Y., S.G., V.S., E.M.W., Z.G., F.M., and W.C. Writing–original draft: L.W.Y., A.L., Y.J., D.N., T.I., and Z.G. Writing–review and editing: L.W.Y., A.L., Y.J., D.N., R.W., Y.L., R.G., X.Z., T.I., V.S., J.L., S.A.M., J.M.M., B.W.M., E.M.W., A.L.J., Z.G., F.M., and W.C. **Competing interests:** The authors declare that they have no competing interests. **Data and materials availability:** All data needed to evaluate the conclusions in the paper are present in the paper and/or the Supplementary Materials.

Submitted 15 April 2025
Accepted 28 October 2025
Published 26 November 2025
10.1126/sciadv.ady2661